Proceedings of the Combustion Institute, 33, pp. 1401-1409, 2011.

Sparse-Lagrangian FDF simulations of Sandia Flame E with density coupling

Yipeng Ge, M.J. Cleary and A.Y. Klimenko

The University of Queensland, School of Mechanical and Mining Engineering, QLD, 4072, Australia

Abstract

Sparse-Lagrangian filtered density function (FDF) simulations are performed for Sandia flame E. A generalised multiple mapping conditioning (MMC) mixing model for the Lagrangian field enforces mixing localisation in the Eulerian large eddy simulation (LES) mixture fraction space. The modelled level of local extinction is determined by the appropriate pairing of mixing particles and the timescale of their mixing interaction. A major development presented in this paper is the inclusion of density coupling between the Eulerian LES and Lagrangian particle fields achieved through use of the equivalent enthalpy method adapted for sparse conditions. Results for two sparse simulation cases, one with one Lagrangian particle per eight Eulerian LES grid cells and the other with one particle per 32 Eulerian LES grid cells, show that accurate FDF predictions of passive and reactive scalars can be achieved for a relatively modest computational cost.

Keywords: filtered density function, sparse-Lagrangian simulations, multiple mapping conditioning

1. Introduction

The concept of the filtered density function (FDF), defined as the probability density function (PDF) of subfilter fluctuations [1], was developed to permit a probabilistic closure of the subfilter scale in large eddy simulations (LES) of turbulent reacting flows. Here we deal with hybrid simulations where the FDF is closed at the joint scalar level and the velocity is simulated by conventional Eulerian LES. The great advantage of FDF methods is that the chemical source terms in the transport equation are treated exactly [2–4]. The numerical implementation employs a stochastic Lagrangian particle method and various mixing models can be used to close the subfilter conditional dissipation term. Within the past five years a number of FDF simulations of target laboratory flames have demonstrated the quality of the method [5–7]. Conventionally the FDF is represented by an ensemble of many Lagrangian particles per Eulerian LES grid cell and this imposes a very high computational cost. We refer to these conventional cases as intensive-Lagrangian simulations, and the opposite case of significantly fewer Lagrangian particles than Eulerian grid cells as sparse-Lagrangian simulations. The notion that the FDF can be represented by very few particles is quite straightforward. Disregarding modelling requirements, if all particles within an ensemble of particles representing the one-point, one-time

FDF are statistically independent, then all particles but one can be removed and that remaining particle (whose value has not changed) is still a characteristic realisation of the FDF. Obviously, in order to evaluate local, instantaneous statistical quantities such as the filtered mean or higher moments more particles are needed but stationary statistical quantities can be accumulated over time using relatively far fewer particles. Alternatively instantaneous statistics can be evaluated over larger physical domains containing many particles. Of course, the option always remains to add more particles to resolve the finer details of the field if needed.

In order for sparse-Lagrangian simulations to produce accurate and useful results we must, of course, consider the modelling implications of using very few particles. The two major modelling implications considered here are localness and evaluation of filtered density. Mixing model performance is very sensitive to the localness of the mixing particles. It has been demonstrated that the major mixing models perform better when particle spacing is small [8] but having sufficient numbers of particles for localness in physical space also imposes a large computational burden. An alternative to a strict enforcement of physical localness are models which mix particles that are close in composition space [9]. Multiple mapping conditioning (MMC) [10] is a PDF/FDF mixing model which makes use of reference (or conditioning) variables to enforce localness in composition space. Additionally the MMC reference variables are independent of the stochastic Lagrangian composition field to also ensure that the mixing is both linear and applied to all scalars equally. For non-premixed combustion the mixture fraction is the simplest, and best example of such a reference variable; proximity in mixture fraction space implies a high degree of localness in composition space and, as it is a conserved scalar, a mathematically independent mixture fraction can be simulated relatively easily. The practical feasibility of sparse-Lagrangian FDF simulations with an MMC closure was demonstrated at the most recent past symposium by simulations of Sandia Flame D using as few as 10,000 reacting particles [11]. Utilising a generalised interpretation of MMC [12], the reference variable is given by the Eulerian LES filtered mixture fraction. Note that MMC is a general modelling framework which is not restricted to the use of a single mixture fraction reference variable. Alternative sensible enthalpy and scalar dissipation reference variables are introduced in Ref.[13].

A weakness in that first sparse-Lagrangian publication [11] is that filtered density is not evaluated from the particle properties and there is no coupling between the Lagrangian and Eulerian fields. This weakness is rectified here. Besides accuracy, any density coupling algorithm must ensure numerical stability of dynamic interactions between Lagrangian and Eulerian submodels. The stability problem exists in intensive-Lagrangian simulations, but it becomes more acute in sparse simulations. The method of equivalent enthalpy, suggested by Muradoglu *et. al.* [14], is highly effective in ensuring stability and accuracy of density feedback in hybrid schemes. The method solves the Eulerian transport equation for an enthalpy-like quantity to determine the density while the influence of Lagrangian values (which can be destabilising when density is directly calculated from them) is restricted to the source term in the Eulerian equation. The equivalent enthalpy method was successfully used in intensive FDF/LES simulations, including simulations of Sandia Flame E [7]. In the present work, we utilise a modification of this method, adapted for the sparse-Lagrangian environment. While the original concept of equivalent enthalpy [14] is a rigorous approach with full consistency of Lagrangian and Eulerian treatments of density, our modification is a model that neglects conditional fluctuations of the density.

The sparse-Lagrangian FDF model with a generalised MMC closure along with the key mixing model parameters are presented in the next section while Section 3 describes the density coupling. The resulting model is tested against experimental data for flame conditions with moderate levels of local extinction and strong temporal and spatial density variations (Sandia piloted jet flame E [15]). This test case configuration and numerical details are found in Section 4 and the results appear in Section 5. Conclusions are drawn in Section 6.

2. The Model

A hybrid method is used consisting of an Eulerian LES for the simulation of filtered velocity, u_j and the filtered mixture fraction, $\widetilde{f}$, coupled with a Lagrangian FDF scheme for the simulation of the composition field, ϕ_α. The LES is formulated for the 3D polar coordinate system [16] with a Smagorinsky turbulent viscosity, ν_t [17], and the dynamic Germano model [18] for the proportionality constant. The subfilter diffusivity in the $\widetilde{f}$ equation is modeled as $D_t = \nu_t/\sigma_t$ where $\sigma_t = 0.4$ [19].

The Lagrangian mass-weighted FDF is solved stochastically according to the equations developed by Jaberi *et al.* [4] and also presented in Ref.[11]. Particles move in physical space with a random-walk component to represent molecular and subfilter diffusion. Particle compositions undergo change due to chemical reaction and conditional scalar dissipation at the subfilter scale. The former is in exact form and requires no additional modelling while the latter is modelled by a particle interaction model similar to Curl's model [20]. At each time step all particles are formed into pairs and mix linearly with a locally evaluated timescale τ_L which determines the rate of decay of subfilter scalar variance. Particle pairs (p and q) are formed such that the normalised square distance in

$(\boldsymbol{x}, \widetilde{f})$-space

$$\tilde{d}^2_{(p,q)} = \frac{1}{1+\lambda^2} \times \left[\sum_{j=1}^{3} \left(\frac{\Delta^{(p,q)} x_j^*}{L_x} \right)^2 + \lambda^2 \left(\frac{\Delta^{(p,q)} \widetilde{f}^*}{L_f} \right)^2 \right] \quad (1)$$

is small. In practice an approximate minimisation of $\tilde{d}^2_{(p,q)}$ is performed as discussed in Ref.[11]. The following notation is adopted in Eq.(1): $\Delta^{(p,q)}(\cdot) = (\cdot)^{(p)} - (\cdot)^{(q)}$; asterisks denote stochastic quantities assigned to or evaluated at the Lagrangian particles; λ is the localisation parameter (larger λ enforces additional localisation in $\widetilde{f}$-space); and L_x and L_f are characteristic physical and reference scales set to the jet nozzle radius and 1.0, respectively. In these MMC calculations there are two different mixture fractions: $\widetilde{f}^*$ is the reference mixture fraction simulated according to conventional Eulerian LES, interpolated to the particle location and used to determine which particles mix; and Z^* is the real mixture fraction consistent with the species concentrations, ϕ_α, and evaluated according to the Lagrangian FDF equations.

For consistency between the Lagrangian and Eulerian fields the models for the explicit particle mixing timescale, τ_L, and the implicit Eulerian mixing timescale, τ_E, must account for the difference in characteristic filter scales for those two fields; Δ_L and Δ_E, respectively. In accordance with the principles of LES it is assumed that both filter widths are within the inertial range and are therefore small relative to the macro lengthscale of the flow. In addition to consistency considerations the model should avoid introducing excessive numerical diffusion which increases as Δ_L^2/τ_L [21]. Previous modelling [11] based on the proportionality of mechanical and mixing timescales in the inertial range gave $\tau_L \sim (\Delta_L/\Delta_E)^{2/3}\tau_E$. That model assumes that variance decays isotropically and homogeneously within a radius Δ_L. An improved model is used here. From the definition of the dissipation timescale as the ratio of scalar variance and scalar dissipation we have $\tau_E = \widetilde{f''^2_E}/\chi$ and $\tau_L = \widetilde{f''^2_L}/\chi$ where $\widetilde{f''^2_E}$ and $\widetilde{f''^2_L}$ are the subfilter variances at scales Δ_E and Δ_L, respectively. Taking χ to be constant within the inertial range it follows that $\tau_L = C_L^{-1}(\widetilde{f''^2_L}/\widetilde{f''^2_E})\tau_E$. The constant C_L is unity although it could in practice be used as an additional parameter to control subfilter fluctuations [11]. Conventional algebraic models are used for $\widetilde{f''^2_E}$ and χ (e.g. Ref.[22]) such that

$$\widetilde{f''^2_E} = C_f \Delta_E^2 \nabla\widetilde{f} \cdot \nabla\widetilde{f} \quad (2)$$

and

$$\chi = 2(D + D_t)\nabla\widetilde{f} \cdot \nabla\widetilde{f} \quad (3)$$

where $C_f = 0.1$. Using the same form as Eq.(2) we model $\widetilde{f''^2_L}$ as

$$\begin{aligned} \widetilde{f''^2_L} &= C_f \Delta_L^2 \nabla\widetilde{f}^* \cdot \nabla\widetilde{f}^* \\ &\approx C_f \Delta_L^2 \beta \left(\frac{\Delta_{(p,q)}\widetilde{f}^*}{\Delta_L} \right)^2 . \end{aligned} \quad (4)$$

Depending on the orientation of the particle pair within the $\widetilde{f}$ field the coefficient β is a number between 1 and 3; the latter value being for homogeneous regions of the flow. Smaller β implies a smaller value of τ_L and for some particle pairs this may induce significant numerical diffusion. Here we set $\beta = 3$ which may lead to a slight over-prediction of Lagrangian subfilter variance at some locations but, unlike a too small value of β, will not produce excessive numerical diffusion which degrades the mean fields. Incorporating Eq.(2) and (4) into the model for τ_L gives

$$\tau_L = C_L^{-1} \frac{\beta \left(\Delta^{(p,q)} \widetilde{f}^* \right)^2}{\Delta_E^2 \nabla\widetilde{f} \cdot \nabla\widetilde{f}} \tau_E. \quad (5)$$

The hybrid model presented above has three parameters: Δ_E, Δ_L and λ. We adopt the common combustion LES approach of linking the filter width to the numerical grid by setting Δ_E to the grid size and similarly Δ_L is taken as the physical distance between the mixing particles. This leaves λ as the only free model parameter. An increase in λ corresponds to greater localisation in the reference mixture fraction space ($\widetilde{f}$) and consequently greater localisation in Z-space. This action results in fewer departures from the conditional mean and hence a decrease in conditional variances. Alternatively, smaller λ implies less localisation in mixture fraction space and an increase in conditional variances. If an FDF model is made more sparse then the spacing between particles increases and, naturally, there is diminished $\widetilde{f}$-space localness of neighbouring particles. The present generalised MMC model allows sparse conditions without a loss of compositional localness by the option of increasing λ as particle spacing increases. This is a strength of the model but it also places a burden on the modeller to correctly select the value of λ. For practical applications an analytical or dynamic model for λ is necessary but such a development will require extensive testing and new theory that is beyond the scope of the present work. Here λ is determined as a universal value throughout the field by *a priori* testing so that the simulated and experimentally observed conditional variances are generally in agreement. Note that the consistency between the Eulerian and Lagrangian scalar fields is ensured even when λ is varied in this way.

3. Density Coupling

For sparse simulations with a density feedback, we face the problem of evaluating the density for

each Eulerian cell from a relatively sparse grid of Lagrangian particles. Our treatment of this problem involves evaluation of conditional averages which are determined using Lagrangian data according to $F(Z;x,t) = \overline{h_s^* | Z^* = \eta}$ and used in Eulerian simulations in the form $F(\widetilde{f};x,t)$. Here h_s denotes equivalent enthalpy [14] which, as discussed below, is related to the density, and η is the sample space variable for mixture fraction. Although our treatment of density is approximate (conditional fluctuations are neglected), conditioning on the mixture fraction is in line with MMC/CMC philosophy and can be expected to produce reasonably good results for non-premixed combustion. Furthermore the adapted equivalent enthalpy method provides numerical stability which a direct coupling method cannot do.

The Eulerian transport equation [14]

$$\frac{\partial \overline{\rho} \widetilde{h_s^E}}{\partial t} + \frac{\partial \overline{\rho} \widetilde{u}_i \widetilde{h_s^E}}{\partial x_i} - \frac{\partial}{\partial x_i}\left[\overline{\rho}\left(D + D_t\right)\frac{\partial \widetilde{h_s^E}}{\partial x_i}\right] = \widetilde{W}_{h_s} \tag{6}$$

is solved for the filtered Eulerian equivalent enthalpy, $\widetilde{h_s^E}$. From it the density is calculated as

$$\overline{\rho} = \frac{\gamma_o}{\gamma_o - 1}\frac{P}{\widetilde{h_s^E}} \tag{7}$$

where γ_0 is the ratio of constant specific heats and P is pressure. Generally, the source term in Eq.(6) can be expressed as a function of gas composition [14] but, unlike in intensive-Lagrangian simulations, we can not directly evaluate it since most of the Eulerian cells do not have any Lagrangian particles. Instead $\widetilde{W}_{h_s}$ is treated as a relaxation term

$$\widetilde{W}_{h_s} = \overline{\rho}\frac{\hat{h}_s - \widetilde{h_s^E}}{\tau_{\text{rel}}} \tag{8}$$

whose job is to dynamically match $\widetilde{h_s^E}$ to a target estimate of the cell-centred value of the Lagrangian equivalent enthalpy, denoted as $\hat{h}_s$ and evaluated as $\hat{h}_s = F(\widetilde{f})$. In principle, more sophisticated conditional approximations for $\widetilde{W}_{h_s}$ can be used but we have found that the simple relaxation equation given by Eq.(8) works reasonably well. The relaxation time, τ_{rel} is determined by numerical conditions: excessively small τ_{rel} can cause instabilities while $\widetilde{h_s^E}$ would deviate from its target $\hat{h}_s$ for excessively large τ_{rel}. In the present simulations τ_{rel} is set to approximately 20 times the characteristic numerical time step. Although conditional fluctuations are neglected in determining the Eulerian density, the pressure and velocity fields are corrected to ensure that mass is conserved.

In practice, the conditional expectation $F(Z;x,t) = \overline{h_s^* | Z^* = \eta}$ is dynamically evaluated by selecting the curve from a precalculated family of curves which provides the best match to the scatter plot of h_s^* vs. Z^* for particles within the near-neighbourhood of the Eulerian cell. Typically the particle ensemble contains between 20 and 80 particles. For simplicity the precalculated curves are created using data from previous simulations although alternative more sophisticated methods could be devised.

4. Simulation Details

The sparse-Lagrangian FDF model with a generalised MMC closure and density coupling is tested for Sandia Flame E [15, 23] which exhibits moderate levels of local extinction and strong temporal and spatial density variations. The burner has a central fuel nozzle of diameter $d = 7.2$mm surrounded by a premixed pilot that extends to a diameter of 18.2mm. The jet fuel is 25% CH_4 and 75% air by volume and has a stoichiometric mixture fraction of $Z_{\text{st}} = 0.351$. The pilot burns a lean premixture with the same nominal enthalpy and equilibrium composition as methane/air at an equivalence ratio of 0.77. The bulk jet velocity is 74.4m/s giving a nominal Reynolds number of 33,600. The pilot inlet velocity is 17.1m/s.

The hybrid Eulerian LES / sparse-Lagrangian FDF model is implemented numerically within the Flowsi LES code [16] as documented in earlier publications [11, 12]. Two model cases with different particle resolutions are simulated. The first, denoted 1L/8E, has a nominal distribution of 1 Lagrangian particle for every 8 Eulerian LES grid cells while the second, denoted 1L/32E, has 1 particle for every 32 cells. The first simulation is for a domain extending axially to $L_{\text{axial}} = 0.25$m (35 jet diameters) with 512 Eulerian grid points while the second simulation extends to $L_{\text{axial}} = 0.5$m using 1024 grid points. Radially and azimuthally there are 55 and 32 Eulerian grid points, respectively. For both simulations the smallest finite volume cells at the axis are 0.5mm$\times$0.5mm$\times\pi/32$ radians. In the 1L/8E cases the characteristic distance between particles at the jet axis is approximately 1mm, and in the 1L/32E case that distance is approximately 1.6mm. The computational cost of these sparse-Lagrangian simulations is relatively very low. Compared to a typical intensive-Lagrangian FDF simulation with 50 particles per LES cell the 1L/8E case has of the order of 400 times fewer particles while 1L/32E has of the order of 1600 fewer particles. The absolute cost is largely determined by the number of reacting particles as inert particles impose only a minor additional load. Here reaction rates are calculated for $0.05 < Z^* < 0.95$ resulting in about 30,000 reacting particles for 1L/8E (35 diameter domain length) and about 20,000 reacting particles for 1L/32E (70 diameter domain length). Once a steady-state is established simulations continue for at least three domain flow through times which requires about five to eight days on a four-processor desktop workstation. Chemical source terms are from a detailed kinetics scheme (GRI-3.0) [24] containing 34 species and 219 reactions (NOx excluded) and time integration is by the stiff ODE solver DVODE [25].

Radiation is modelled for the optically thin assumption with absorption coefficients given in Ref. [26].

An artefact of some Eulerian LES schemes when applied to jet flames is the appearance of a local velocity fluctuation maxima between 5 and 10 diameters downstream of the nozzle which does not coincide with experimental data [27]. As reactive species predictions can be sensitive to these velocity fluctuations it is necessary to reduce them as far as possible. It is reported that locating the numerical inflow plane upstream of the nozzle exit is an effective measure against these spurious fluctuations [27]. Here we have opted for a simple and less computationally expensive intervention which consists of filtering the density over immediately adjacent grid cells before calculating $\partial\rho/\partial t$ in the pressure solver. This filtering is not applied to other terms involving density and nor is the stability of the density coupling method reliant upon it.

5. Results

A series of about five *a priori* simulations were performed for both 1L/8E and 1L/32E to determine appropriate values of λ based on a satisfactory match between predictions of reactive scalars and the experimental data. As discussed above λ controls the level of conditional fluctuations with larger λ resulting in smaller conditional variances. For the 1L/8E simulation case it was found that $\lambda = 15$ produces a satisfactory agreement while for the 1L/32E case $\lambda = 44$ is required. Unless otherwise noted results below are presented for those values of λ. A scaling analysis may be useful for predicting the correct value of λ when the spacing between particles varies. Assuming that $\Delta^{(p,q)}\widetilde{f}^*$ and τ_L are kept constant between simulations then it can be shown that $\lambda_2/\lambda_1 = (n_1/n_2)^{\frac{3}{8}}$ where n is the number of particles [28]. Taking $\lambda = 15$ for 1L/8E is the starting point we would expect $\lambda \sim 25$ for 1L/32E. The discrepancy with the required value of $\lambda = 44$ is probably due to incorrect assumptions in the scaling. In the present modelling τ_L is a function of $\Delta^{(p,q)}\widetilde{f}^*$ and is unlikely to be the same for both cases. Improved scaling analysis may be useful in future attempts to develop a closed form model for λ.

The initial task is to demonstrate the density coupling between the Lagrangian and Eulerian fields. As discussed in Section the model enforces consistency of conditional density between the Eulerian and Lagrangian fields. This is demonstrated in Fig.1 showing excellent agreement between the Lagrangian and Eulerian time-averaged conditional density at $x/d = 15$. Results at other locations are similarly consistent.

Figure 2 shows radial profiles of the experimental and the Lagrangian and Eulerian simulated average and rms mixture fraction at various axial locations. Both the 1L/8E and 1L/32E Lagrangian predictions are generally in very good agreement with experimental data, although there is small under-prediction of the mean at the outer edge of the shear layer. The Lagrangian results are noticeably better than the Eulerian mixture fraction predictions which tend to be excessively diffusive. The Lagrangian and Eulerian mixture fraction fields are topologically similar despite those apparent small differences and hence the quality of the the Eulerian mixture fraction $\widetilde{f}$ as a reference variable for localisation of mixing is unlikely to be diminished. The accuracy of the Lagrangian results despite a relatively large distance between particles is attributed to the mixing timescale model given by Eq.(5). This model adjusts τ_L so that the rate of decay of Lagrangian scalar variance matches the Eulerian LES while also accounting for the increased length scale in the Lagrangian field relative to that in the Eulerian field.

Figure 3 shows scatter plots of temperature versus mixture fraction at $x/d = 15$. Both simulations capture the extent and distribution of local extinctions and reignitions very well at this location. The conditional mean and rms of temperature at this location and also at $x/d = 7.5$ and 30 are shown in Fig.4. These are for 1L/8E with $\lambda = 15$ and 1L/32E with $\lambda = 44$ with an additional result for 1L/32E with $\lambda = 50$ included. This latter result demonstrates how λ controls conditional variances. An increase in λ from 44 to 50 for 1L/32E enforces additional localisation in $\widetilde{f}$-space resulting in a lower level of fluctuations relative to the conditional mean and hence the extent of extinctions is diminished. Clearly, for the 1L/32E simulation $\lambda = 44$ produces more accurate results than does $\lambda = 50$. The remainder of the discussion deals with the primary simulation cases only: 1L/8E with $\lambda = 15$ and 1L/32E with $\lambda = 44$. At $x/d = 7.5$ 1L/8E under-predicts the level of extinctions and hence the conditional mean temperature near stoichiometry is over-predicted while the conditional rms is under-predicted. In contrast 1L/32E is in very good agreement with experimental data at $x/d = 7.5$. By the next axial station, $x/d = 15$, where the level of extinctions remains high the 1L/8E predictions are in good agreement with both the experimental data and the 1L/32 simulation results. The flame exhibits strong reignition by $x/d = 30$ and this is captured quite well by both 1L/8E and 1L/32E. It appears that the axial location of the heaviest extinctions is delayed in the 1L/8E simulation relative the experimental data whereas 1L/32E captures this location quite well. A reduction in λ below 15 for 1L/8E could produce more accurate results close to the nozzle but would also lead to excessive extinction further downstream where there is currently good agreement with experimental data. This issue is further discussed at the end of the section.

Figure 5 shows conditional mean profiles of selected major and intermediate reactive species at $x/d = 7.5$, 15 and 30. The species predictions are consistent with those for conditional temperature discussed above. 1L/8E under-predicts the level of extinctions at $x/d = 7.5$ and the higher temperatures near stoichiometry lead to excessive residual O_2

while rich side CO and H_2 are over-predicted. At the axial locations further downstream 1L/8E species predictions are in good agreement with the experimental data. In contrast 1L/32E species results are quite good at all locations and especially at $x/d = 7.5$ where this simulation captures the level of extinctions very well. It is noted that both simulation cases slightly over-predict rich side conditional CO and H_2 although this is comparable to predictions of those species in previously published results [7]. While we have not conducted a detailed analysis, we can note that temperature and major species are very good at the same locations and therefore the source of the intermediate species error may be in the chemical kinetics.

Radial profiles of the unconditional means of selected reactive species are shown in Fig.6. The results are consistent with the earlier observations for mean mixture fraction and conditional mean species. The greatest discrepancy with experimental data occurs for 1L/8E at $x/d = 7.5$ and generally in the outer part of the shear layer where the cause is an under-prediction of mixture fraction as discussed above.

A couple of general comments can be made from the temperature and species results. The first is that, as expected. λ can be adjusted to vary the level of conditional variances without affecting the consistency between the mixing fields (c.f. Fig. 2). With increased distances between mixing particles λ should be increased to enforce mixture fraction localisation and to overcome the excessive conditional fluctuations that would otherwise be present (these are due to numerical diffusion which increases with distance between particles). It is noted that for the present simulations the case with higher particle resolution, 1L/8E, does not necessarily produce the best results. With more particles the finer details of the turbulent fields are simulated. Close to the nozzle the shear layer where extinctions occur is very thin and with a greater number of particles 1L/8E is probably reflecting the true nature of the current sparse-FDF model better than the 1L/32E case can only model equivalent statistics of the fine scale distributions. We note that even in Eulerian LES a reduction in filter width does not necessarily lead to a smaller total error [29]. The 1L/8E results indicate that while $\lambda = 15$ is satisfactory at many locations, reactive species predictions are sensitive to the value and it may not be constant for all locations in the flow (e.g. a value lower than 15 appears to be needed close to the nozzle). This reinforces the need to develop a model for λ if the method is to be useful for practical applications.

6. Conclusion

A sparse-Lagrangian FDF model with a generalised MMC closure is tested against experimental data of a piloted jet flame with moderate levels of local extinction. The major advance, over earlier publications, is the inclusion of a stable density coupling scheme based on the equivalent enthalpy method. The instantaneous conditional fluctuations of density are neglected but the conditional average densities of the Lagrangian and Eulerian fields are fully consistent. Ongoing research indicates that the model is robust and numerically stable even for simulations leading to global extinction.

Two sparse simulation cases are presented: the first having nominally 1 Lagrangian particle per 8 Eulerian LES cells and the second having 1 Lagrangian particle per 32 Eulerian LES cells. The simulations yield reasonably accurate conditional and unconditional statistics of the passive and reactive scalars, although it is shown that the latter are sensitive to the correct selection of a localisation parameter, λ, which is currently selected by *a priori* simulations. The level of control afforded by λ is a strength of the model, but, to complete the model it will be necessary to develop an analytical or dynamic model for λ. This step will require extensive testing and theoretical analysis over a range of conditions. Here we have demonstrated that suitable values of λ exist for two models with different levels of sparseness: $\lambda = 15$ for 1L/8E and $\lambda = 44$ for 1L/32E.

The attraction of sparse-Lagrangian FDF simulations is their modest computational cost relative to conventional intensive-Lagrangian FDF simulations. The cost of the present sparse simulations is two to three orders of magnitude lower than conventional intensive FDF simulations of the same flame [7]. The quality of the sparse predictions is comparable to those for intensive simulations although, of course, the finest details of the fields are not reproduced to the same extent.

References

[1] S.B. Pope, *Proc. Combust. Inst.* , 23 (1990) 591-612.

[2] F. Gao, E.E. O'Brien, *Phys. Fluids A* 5 (1993) 1282–1284.

[3] P.J. Colluci, F.A. Jaberi, P. Givi, S.B. Pope, *Phys. Fluids* 10 (2) (1998) 499–515.

[4] F.A. Jaberi, P.J. Colucci, S. James, P. Givi, S.B. Pope, *J. Fluid Mech.* 401 (1999) 85–121.

[5] M.R.H. Sheikhia, T.G. Drozda, P. Givi, F.A. Jaberi, S.B. Pope, *Proc. Combust. Inst.* 30 (2005) 549–556.

[6] V. Raman, H. Pitsch and R.O. Fox, *Combust. Flame* 143 (2005) 56–78. (2005).

[7] V. Raman, H. Pitsch, *Proc. Combust. Inst.* 31 (2007) 1711–1719.

[8] F. Bisetti, J.Y. Chen, A. Kempf, J. Janicka, in TNF-8 (Turbulent Nonpremixed Flames) Workshop, Heidelberg, 2006.

[9] S. Subramaniam, S.B. Pope, *Combust. Flame* 115 (1998) 487–514.

[10] A.Y. Klimenko, S.B. Pope, *Phys. Fluids* 15 (2003) 1907–1925.

[11] M.J. Cleary A.Y. Klimenko, J. Janicka, M. Pfitzner, *Proc. Combust. Inst.* 32 (2009) 1499–1507.

[12] M.J. Cleary, A.Y Klimenko, *Flow, Turbulence and Combustion* 82 (2009) 477–491.

[13] A. Kronenburg, M.J. Cleary,*Combust. Flame* 155 (2008) 215–231.

[14] M. Muradoglu, S.B. Pope, D.A. Caughey, *J. Comput. Phys.* 172 (2001) 841–878.

[15] R.S. Barlow, J. Frank, *Proc. Combust. Inst.* 27 (1998) 1087–1095.

[16] A. Kempf, A. Sadiki, J. Janicka, *Proc. Combust. Inst.* 29 (2002) 1979–1985.
[17] J. Smagorinsky, *Monthly Weather Review 1* 91 (1963) 99–164.
[18] M. Germano, U. Piomelli, P. Moin, W. Cabot, *Phys. Fluids A* 3 (1991) 1760–1765.
[19] H. Steiner, H. Pitsch, *Phys. Fluids* 12 (2000) 2541–2554.
[20] R.L. Curl, R.S. Miller, J.L. Ralph, G.D. Towell, *AIChE Journal* 9 (1963) 175–181.
[21] A.Y. Klimenko, *Phys. Fluids* 19 (2007) 31702.
[22] S. Navarro-Martinez, A. Kronenburg, F. Di Mare, *Flow, Turbulence and Combustion* 75 (2005) 245–274.
[23] Ch. Schneider, A. Dreizler, J. Janicka, E.P. Hassel, *Combust. Flame* 135 (2003) 185–190.
[24] http://www.me.berkeley.edu/gri_mech/
[25] P.N. Brown, G.D. Byrne, A.C. Hindmarsh, *SIAM J. Sci. Stat. Comput.* 10 (1989) 1038–1051.
[26] R.S. Barlow, A.N. Karpetis, J.H. Frank, J.Y. Chen, *Combust. Flame* 127 (2001) 2101–2118.
[27] A.W. Vreman, B.A. Albrecht, J.A. van Oijena, L.P.H. de Goey, R.J.M. Bastiaans, *Combust. Flame* 153 (2008) 394–416.
[28] A.Y. Klimenko, M.J. Cleary, *Flow. Turbul. Combust.* submitted 2010.
[29] J. Meyers, B. Geurts, P. Sagaut, *Journal of Computational Physics* 227 (2007) 156–173.

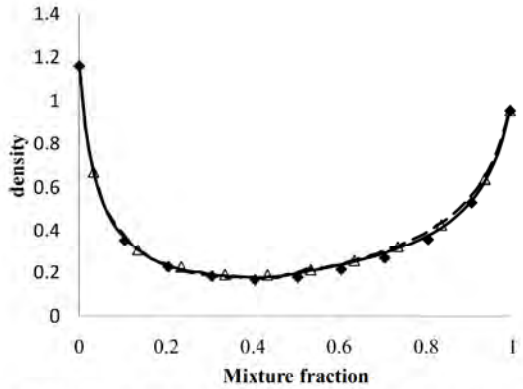

Fig. 1: Conditional density profiles at $x/d = 15$. Closed symbols - $\langle \overline{\rho} | \widetilde{f} = \eta \rangle$ for 1L/8E; solid lines - $\langle \rho^* | Z^* = \eta \rangle$ for 1L/8E; open symbols - $\langle \overline{\rho} | \widetilde{f} = \eta \rangle$ for 1L/32E; dashed lines - $\langle \rho^* | Z^* = \eta \rangle$ for 1L/32E.

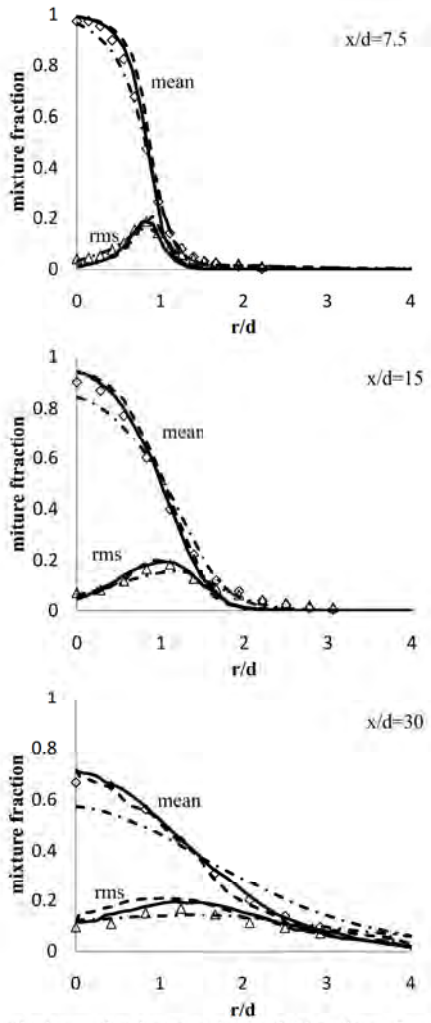

Fig. 2: Radial profiles of mean and rms of mixture fraction at various axial locations. Symbols - experimental data; solid lines - 1L/8E Lagrangian field results; dashed lines - 1L/32E Lagrangian field results; dashed-dotted lines - Eulerian field results.

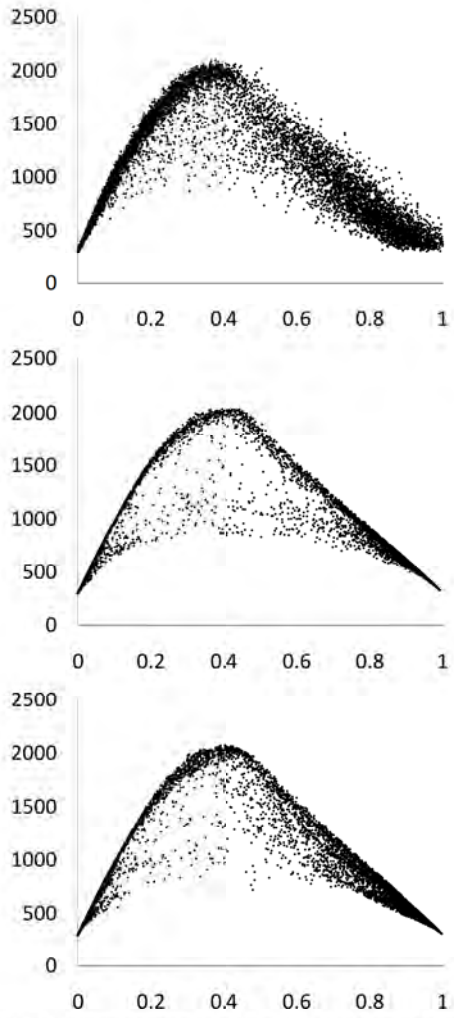

Fig. 3: Scatter plots of temperature versus mixture fraction at $x/d = 15$. Top figure shows experimental data, middle figure is for 1L/8E with $\lambda = 15$ and bottom figure is for 1L/32E with $\lambda = 44$.

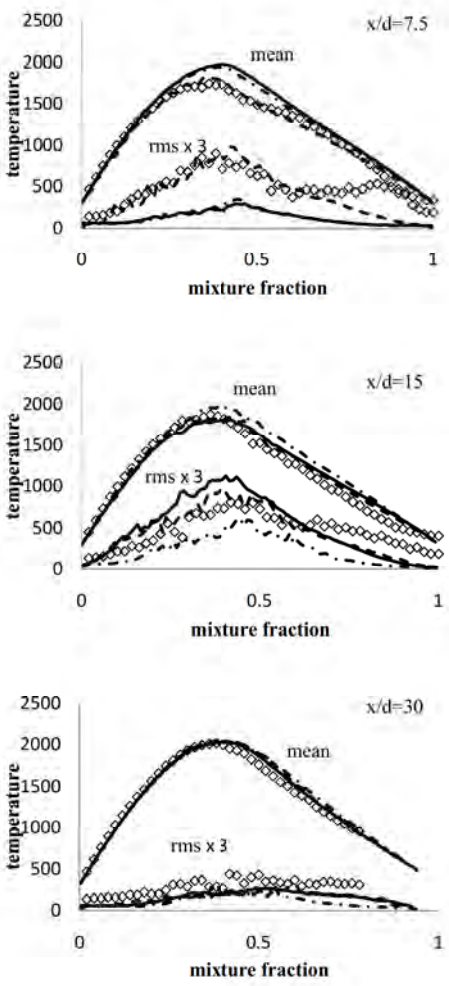

Fig. 4: Conditional temperature profiles at various axial locations. Symbols - experimental data; solid lines - 1L/8E with $\lambda = 15$; dashed lines - 1L/32E with $\lambda = 44$; dashed-dotted lines - 1L/32E with $\lambda = 50$.

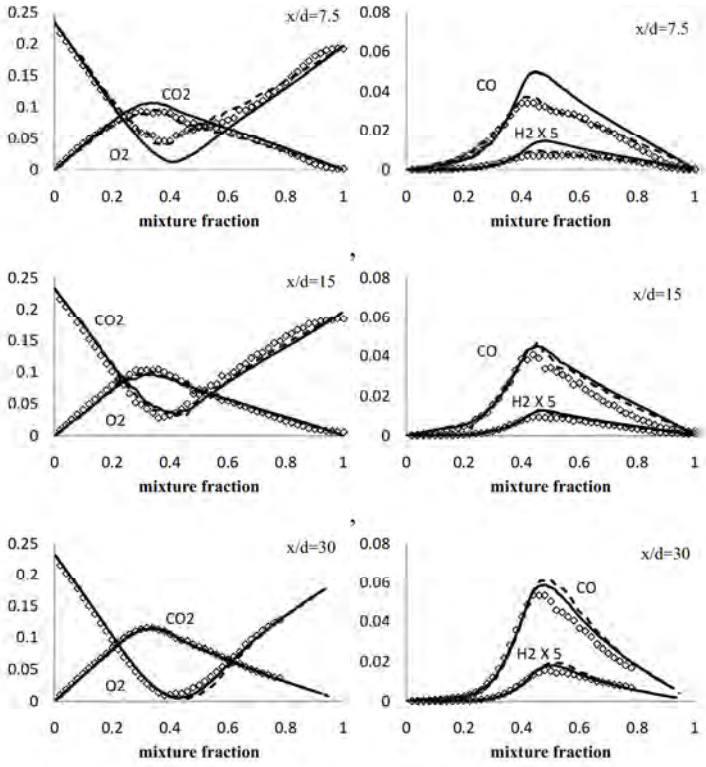

Fig. 5: Conditional profiles of selected reactive species at various axial locations. Symbols - experimental data; solid lines - 1L/8E with $\lambda = 15$; dashed lines - 1L/32E with $\lambda = 44$.

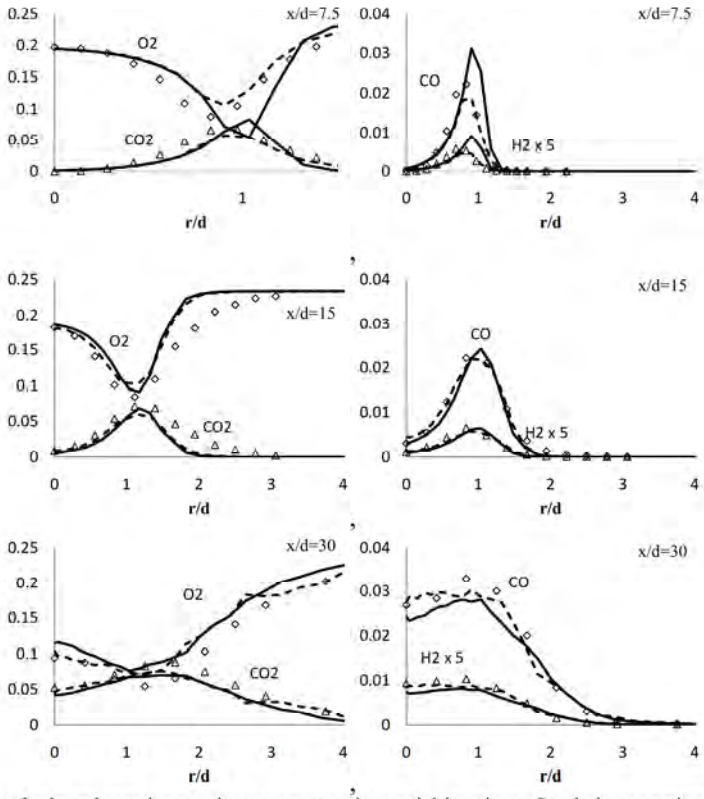

Fig. 6: Radial profiles of selected reactive species means at various axial locations. Symbols - experimental data; solid lines - 1L/8E with $\lambda = 15$; dashed lines - 1L/32E with $\lambda = 44$.